SIAM J. IMAGING SCIENCES
Vol. 3, No. 3, pp. 277–299

A Multiphase Image Segmentation Method Based on Fuzzy Region Competition*

Fang Li†, Michael K. Ng‡, Tie Yong Zeng§, and Chunli Shen†

Abstract. The goal of this paper is to develop a multiphase image segmentation method based on fuzzy region competition. A new variational functional with constraints is proposed by introducing fuzzy membership functions which represent several different regions in an image. The existence of a minimizer of this functional is established. We propose three methods for handling the constraints of membership functions in the minimization. We also add auxiliary variables to approximate the membership functions in the functional such that Chambolle's fast dual projection method can be used. An alternate minimization method can be employed to find the solution, in which the region parameters and the membership functions have closed form solutions. Numerical examples using grayscale and color images are given to demonstrate the effectiveness of the proposed methods.

Key words. multiphase, image segmentation, region competition, fuzzy membership function, alternative minimization

AMS subject classifications. 65K10, 68U10, 90-08

DOI. 10.1137/080736752

1. Introduction.

Image segmentation plays a very important role in computer vision. The aim is to partition an image into several regions so that each region has uniform characteristics such as edges, intensities, color, and texture. In the past decade, this problem has been extensively studied with variational methods and partial differential equations (PDEs). The snake model [13] and the geodesic active contour model [4] use edge detection functions and evolve the curve toward a sharp gradient. However, the edge based method is not robust to noise, and generally a noisy image has to be smoothed. Region based methods incorporate region and boundary information and are robust to noise. One of the most well-known region based methods is the Mumford–Shah model [18], which approximates an image by a piecewise smooth function with regular boundaries. The difficulty in studying the Mumford–Shah functional is that it involves two unknowns: the intensity function and the set of edges. The Mumford–Shah model is hard to implement in practice since the discretization of the unknown set of edges is a very complex task. A commonly used method is to approximate the Mumford–Shah functional by a sequence of regular functionals defined on Sobolev spaces, which converges to the Mumford–Shah functional in the sense of Γ-convergence [1]. In the

*Received by the editors September 30, 2008; accepted for publication (in revised form) April 13, 2010; published electronically July 13, 2010. This research was supported in part by RGCs 201508 and 203109, HKBU FRGs, the Research Fund for the Doctoral Program of Higher Education (200802691037), the Natural Science Foundation of Shanghai (10ZR1410200), and the Natural Science Foundation of China (60773119, 10971066).
http://www.siam.org/journals/siims/3-3/73675.html
†Department of Mathematics, East China Normal University, Shanghai 200062, China (lifangswnu@126.com, cshen@math.ecnu.edu.cn).
‡Corresponding author. Centre for Mathematical Imaging and Vision and Department of Mathematics, Hong Kong Baptist University, Kowloon Tong, Hong Kong (mng@math.hkbu.edu.hk).
§Department of Mathematics, Hong Kong Baptist University, Kowloon Tong, Hong Kong (zeng@hkbu.edu.hk).

regular functionals, the set of edges does not appear. The special case of the piecewise constant Mumford–Shah model is studied by Chan and Vese [5] and Chan, Sandberg, and Vese [7] using the level set method [21]. Zhu and Yuille [24] proposed a region competition method by unifying snake, region growing, and Bayesian statistics. This method penalizes the length of the boundaries and the Bayesian error within each region. The error is estimated by parametric probability distributions such as Gaussian distribution. Then the piecewise constant Mumford–Shah model can be regarded as a special case of the region competition method. Curve evolution techniques are used in the implementation of region competition.

Multiphase segmentation is a more challenging problem than two-phase segmentation. The main difficulty is in finding effective representations of the regions and their boundaries. Several recent works are related to the multiphase Mumford–Shah model. Vese and Chan [23] generalized the two-phase model [5] to multiphase segmentation by using multiple level set functions. Both piecewise constant and piecewise smooth cases are studied. The advantage of using level set functions to represent the regions is that it automatically avoids the problems of vacuum and overlap. However, this method has several disadvantages: (i) The numerical solution of the level set equation is obtained by the gradient descent method which converges slowly, and the iterate is in the trap of a local minimum. (ii) For numerical stability, the level set function should be reinitialized periodically as the sign distance function. (iii) Multiple regions cannot be handled in a straightforward manner. The evolution equation of the level set functions is so difficult to unify that one must write down the equation for each level set, which is a tedious task.

Samson et al. [20] proposed another level set based multiphase segmentation model by adding a penalty term on the level set functions to penalize the vacuum and overlap. We note that their idea inspires our proposed method for dealing with the summation to one constraint of membership functions. In this formulation, the multiple regions can be handled directly. However, the numerical disadvantages of local minima and reinitialization of the level set function still remain. Lie, Lysaker, and Tai [15] proposed using binary level set functions which take value 1 or -1 instead of using the classical continuous level set functions in the piecewise constant Mumford–Shah segmentation framework. A smooth convex functional with a quadratic constraint is minimized, and no reinitialization of the level set function is needed. Then, Lie, Lysaker, and Tai [16] introduced a piecewise constant level set function and used each constant value to represent a unique phase in a piecewise constant segmentation model. Their approach has difficulties in representing the unit normal and the mean curvature for the curves, which is easily done by the classical level set. Another disadvantage of their method is the sensitivity to the initial guess. Jung, Kang, and Shen [12] proposed a phase field method to handle multiphase piecewise constant segmentation. The method is based on the phase transition model of Modica and Mortola with a sinusoidal potential. Since the model is not quadratic or convex, a convex-concave procedure is used in the implementation. The Γ-convergence behavior of their model and the existence of its minimizers are established. Chung and Vese [9] proposed a multilayer approach for multiphase piecewise constant segmentation. In their method, several level lines of the same level set function are used to represent the boundaries of regions, which have the property that one region is a subset of another. It takes almost an entire page to write down the evolution equation of two level set functions with m and n layers, respectively.

Different from the above-mentioned methods which yield hard segmentation results, fuzzy segmentation approaches are popular in data mining and medical image segmentation [2]. In the fuzzy method, it is assumed that each image pixel can be associated with several regions. The probability is represented by fuzzy membership functions valued in [0,1]. Recently, many two-phase fuzzy segmentation models have been proposed [6, 3, 17, 10], in which one fuzzy membership function is used in the functionals such that the functionals are convex with respect to the membership. The convexity ensures that the new methods are not sensitive to initialization, making it possible for global minima to be found. Another advantage is that Chambolle's fast dual projection method [8] can be adopted in the implementation. However, this technique is used only in two-phase segmentation. Extension of this framework to multiphase segmentation is not trivial. A general multiphase stochastic variational soft segmentation model was proposed by Shen [22] based on the Mumford–Shah model. To represent the ownership of each class, Shen used stochastic variables (such as fuzzy membership functions) which are regularized by a regularization term with a double well potential related to the phase field. However, the energy functional in this model is nonconvex with respect to each stochastic variable. Moreover, a set of PDEs of the stochastic variables has to be solved, which makes the implementation computationally expensive.

In this paper, we develop and study a multiphase image segmentation method based on fuzzy region competition. The new variational functional is obtained by introducing fuzzy membership functions in the original region competition functional. The existence and symmetry of minimizers of this new functional are established. We need to minimize the functional under two convex constraints of membership functions. Three methods are proposed to handle the constraints in the minimization procedure. The Karush–Kuhn–Tucker (KKT) conditions can be applied in one of the methods. We also add auxiliary variables to approximate the membership functions in the functional such that Chambolle's fast dual projection method can be used. Meanwhile, the membership functions have closed form solutions. An alternate minimization method can be employed to find the solution of the problem. Numerical examples with grayscale and color images are given to demonstrate the promising results of the proposed methods.

The outline of this paper is as follows. In section 2, we review related works. In section 3, we propose and analyze our model. In section 4, we present our algorithm. In section 5, an extension to vector-valued images is considered. In section 6, we present experimental results to illustrate the effectiveness of our model. Concluding remarks are given in section 7.

2. Related works.

The segmentation problem can be formulated as follows: Given a grayscale image $I : \Omega \to \mathbb{R}$, where the image domain Ω is a bounded and open subset of $\mathbb{R}^2$, the aim is to partition Ω by certain suitable measures into N regions $\{\Omega_i\}_{i=1}^N$ such that $\Omega_i \bigcap \Omega_j = \emptyset, j \neq i$, and $\bigcup_{i=1}^N \Omega_i = \Omega$.

2.1. Mumford–Shah model.

Mumford and Shah [18] proposed solving the segmentation problem by minimizing the following energy:

$$E_{MS}(g,\Gamma) = \lambda \int_\Omega (I-g)^2 dx + \mu \int_{\Omega-\Gamma} |\nabla g|^2 dx + |\Gamma|, \tag{2.1}$$

where $\Gamma = \bigcup \partial\Omega_i$ is the union of boundaries of Ω_i, $|\Gamma|$ denotes the arc length of curve Γ, and λ, μ are the weight parameters. The interpretation of the three terms is as follows: The first term requires that g approximates I; the second term requires that g does not vary much on each Ω_i; and the third term requires that the boundary Γ be as short as possible. Here, g is a piecewise smooth approximate function of image I. In particular, Mumford and Shah considered the special case where the function g is chosen to be a piecewise constant function.

2.2. Chan–Vese model. The piecewise constant Mumford–Shah model was studied by Chan and colleagues using the level set method [5, 7, 23]. Chan and Vese [5] proposed the following minimization method for two-phase segmentation:

$$\min\left\{E_{CV}(\Gamma, c_1, c_2) = \mu|\Gamma| + \lambda_1 \int_{inside(\Gamma)} |I - c_1|^2\, dx + \lambda_2 \int_{outside(\Gamma)} |I - c_2|^2\, dx\right\}.$$

In the level set method [21], $\Gamma \subset \Omega$ is represented by the zero level set of a Lipschitz function $\phi : \Omega \to \mathbb{R}$, such that

$$\begin{cases} \Gamma = \{x \in \Omega : \phi(x) = 0\}, \\ inside(\Gamma) = \{x \in \Omega : \phi(x) > 0\}, \\ outside(\Gamma) = \{x \in \Omega : \phi(x) < 0\}. \end{cases}$$

Then the level set formulation of the Chan–Vese model is

$$\min\left\{\begin{array}{c} E_{CV}(\phi, c_1, c_2) = \mu \int_\Omega |\nabla H(\phi)|\, dx \ + \lambda_1 \int_\Omega |I - c_1|^2 H(\phi) dx \\ + \lambda_2 \int_\Omega |I - c_2|^2 (1 - H(\phi))\, dx \end{array}\right\}, \tag{2.2}$$

where $H(\phi)$ is the Heaviside function: $H(\phi) = 1$ if $\phi \geq 0$ and $H(\phi) = 0$ otherwise. The evolution equation of ϕ is

$$\frac{\partial \phi}{\partial t} = \delta_\varepsilon(\phi)\left(\mu \mathrm{div}\left(\frac{\nabla \phi}{|\nabla \phi|}\right) - \lambda_1 (I - c_1)^2 + \lambda_2 (I - c_2)^2\right), \tag{2.3}$$

where $\delta_\varepsilon(\phi)$ is an approximation of the Dirac function $\delta(\phi)$ and c_1, c_2 are updated by the formula

$$c_1 = \frac{\int_\Omega I H(\phi) dx}{\int_\Omega H(\phi) dx}, \qquad c_2 = \frac{\int_\Omega I\,(1 - H(\phi))\, dx}{\int_\Omega (1 - H(\phi))\, dx}. \tag{2.4}$$

The Chan–Vese model is extended to the multiphase case in [7] which can deal with 2^n-phase segmentation using n level set functions. The corresponding formula is quite complicated and is omitted here.

2.3. Region competition. Zhu and Yuille [24] proposed minimizing the following energy:

$$F(\Gamma, \{\alpha_i\}) = \sum_{i=1}^{N} \left\{\frac{\mu}{2} \int_{\partial\Omega_i} ds - \int_{\Omega_i} \log P_i(I|\alpha_i) dx\right\}. \tag{2.5}$$

The first term within the braces is the length of the boundary curve $\partial\Omega_i$ for region Ω_i. $\Gamma = \bigcup_{i=1}^{N} \partial\Omega_i$ represents the segmentation boundaries of the entire image. The second term

is the sum of the cost for coding the intensity I into region Ω_i by the conditional probability distributions $-\log P_i(I|\alpha_i)$, where α_i is the parameter in the probability density function P_i.

A general two-phase region competition problem is minimizing

$$F(\Gamma, \alpha_1, \alpha_2) = \int_{\partial\Omega_1} ds + \lambda \int_{\Omega_1} r_1(I, \alpha_1)dx + \lambda \int_{\Omega_2} r_2(I, \alpha_2)dx,$$

where the image region Ω is partitioned into Ω_1 and Ω_2, α_i is the region parameter of the region R_i, and $r_i(I, \alpha_i)$ is the error function. To solve the problem, Mory and Ardon [17] proposed using fuzzy membership function $u \in BV_{[0,1]}(\Omega)$ to represent the region and minimize the two-phase fuzzy region competition energy instead:

$$F(u, \alpha_1, \alpha_2) = \int_\Omega |\nabla u|dx + \lambda \int_\Omega r_1(I, \alpha_1)udx + \lambda \int_\Omega r_2(I, \alpha_2)(1-u)dx. \tag{2.6}$$

The fast dual projection method proposed by Chambolle [8] is used to solve the problem.

3. The proposed method. We first write the general N-phase region competition functional as

$$F(\mathcal{R}, \alpha) = \sum_{i=1}^{N} \left\{ \int_{\partial\Omega_i} ds + \lambda \int_{\Omega_i} r_i(I, \alpha_i)dx \right\}, \tag{3.1}$$

where $\mathcal{R} = (\Omega_1, \ldots, \Omega_N)$, $\alpha = (\alpha_1, \ldots, \alpha_N)$, and $r_i(I, \alpha_i)$ are error functions in region Ω_i. Three typical error functions exist in the literature as follows:

1. Chan–Vese model: $r_i(I, \alpha_i) = (I - c_i)^2$, $\alpha_i = c_i$ are constants.
2. Region competition model: $r_i(I, \alpha_i) = -\log P_i(I|\alpha_i)$. For example, if we choose the Gaussian kernel
$$P_i(I|\alpha_i) = \frac{1}{\sqrt{2\pi}\sigma_i} \exp\left(-\frac{(I-\mu_i)^2}{2\sigma_i^2}\right),$$
then $\alpha_i = (\mu_i, \sigma_i)$ are scalars.
3. Mumford–Shah model: $r_i(I, \alpha_i) = (I - s_i)^2 + \mu|\nabla s_i|^2$, where $\alpha_i = s_i$ are functions.

In terms of characteristic functions $\chi = (\chi_1, \ldots, \chi_N)$, where χ_i denotes the characteristic function of region Ω_i, the energy (3.1) can be rewritten as

$$E(\chi, \alpha) = \sum_{i=1}^{N} \left\{ \int_\Omega |\nabla \chi_i|dx + \lambda \int_\Omega r_i(I, \alpha_i)\chi_i dx \right\}. \tag{3.2}$$

The term $\int_\Omega |\nabla \chi_i|dx$ equals the perimeter of Ω_i. There is a scaling of factor 2 since we add each boundary twice. For simplicity, we neglect the factor in the following discussion.

Binary value functions $\{\chi_i\}$ give a hard segmentation of Ω. In the following, we use a fuzzy membership function $u_i(x)$ to substitute the hard membership function χ_i in (3.2). Then, we get our fuzzy region competition segmentation model of minimizing the energy functional

$$E(U, \alpha) = \sum_{i=1}^{N} \left\{ \int_\Omega |\nabla u_i|dx + \frac{\lambda}{p} \int_\Omega r_i(I, \alpha_i)u_i^p dx \right\} \tag{3.3}$$

subject to

$$\text{(i)} \quad \sum_{i=1}^{N} u_i = 1, \quad \text{(ii)} \quad 0 \le u_i \le 1 \text{ for } i = 1, \dots, N,$$

where λ, p are positive parameters and p determines the fuzziness of segmentation.

3.1. Mathematical analysis. Here we choose the Chan–Vese error function $r_i(I, \alpha_i) = (I - c_i)^2$. Under the assumption that the image $I \in L^\infty(\Omega)$, the energy (3.3) is well defined and finite for the admissible set

$$\text{adm}_N = \{U, c | u_i \in BV(\Omega),\ i = 1 : N,\ \text{satisfies (i) and (ii)},\ c \in \mathbb{R}^N\}.$$

In the following we prove the existence and symmetry of minimizers of energy E.

Theorem 3.1 (existence). *Assume that the image $I \in L^\infty(\Omega)$, $I \ge 0$. Then for fixed parameters N, λ, p, there exists a minimizer of the energy E in admissible set* adm_N.

Proof. We let $u_1 = 1,\ u_j = 0,\ j = 2, \dots, N$, and $c_1 = \int_\Omega I dx/|\Omega|,\ c_j = 0,\ j = 2, \dots, N$; then $E(U, c) = \int_\Omega (I - c_1)^2 dx < \infty$. Thus the infimum of the energy must be finite. Let $(U^n, c^n) \subseteq \text{adm}_N$ be a minimizing sequence for energy (3.3); that is, $E(U^n, c^n) \to \inf E(U, c)$ as $n \to \infty$. Then, there exists a constant $M > 0$ such that

$$E(U^n, c^n) = \sum_{i=1}^{N} \left\{ \int_\Omega |\nabla u_i^n| dx + \frac{\lambda}{p} \int_\Omega (I - c_i^n)^2 (u_i^n)^p dx \right\} \le M.$$

Then we have that each term of $E(U^n, c^n)$ is bounded; i.e.,

$$\frac{\lambda}{p} \int_\Omega (I - c_i^n)^2 (u_i^n)^p dx \le M, \tag{3.4}$$

$$\int_\Omega |\nabla u_i^n| dx \le M. \tag{3.5}$$

Since u_i^n satisfies condition (i), $\|u_i^n\|_{L^1(\Omega)} = \int_\Omega u_i^n dx \le |\Omega|$. Together with (3.5) we get that $\{u_i^n\}$ is uniformly bounded in $BV(\Omega)$ for each $i = 1, \dots, N$. By the compactness property of BV space with respect to BV_w^* topology, up to a subsequence also denoted by $\{u_i^n\}$ after relabelling, there exists a function $u_i^* \in BV(\Omega)$ such that

$$\begin{aligned} &u_i^n \to u_i^* \ \text{ strongly in } L^1(\Omega), \\ &u_i^n \to u_i^* \ \text{ a.e. } x \in \Omega, \\ &\nabla u_i^n \rightharpoonup \nabla u_i^* \ \text{ in the sense of measure.} \end{aligned}$$

Then by the lower semicontinuity of total variation,

$$\int_\Omega |\nabla u_i^*| dx \le \liminf_{n \to \infty} \int_\Omega |\nabla u_i^n| dx. \tag{3.6}$$

Meanwhile since u_i^n satisfies constraints (i) and (ii), by the convergence result, u_i^* also satisfies (i) and (ii).

It is easy to derive from the Euler–Lagrange equation of energy E that

$$c_i = \frac{\int_\Omega I(x)u_i^p(x)dx}{\int_\Omega u_i^p(x)dx}$$

if $\int_\Omega u_i^p(x)dx > 0$. Otherwise, if $\int_\Omega u_i^p(x)dx = 0$, we define $c_i = 0$. Then c_i^n is given by

$$c_i^n = \frac{\int_\Omega I(u_i^n)^p dx}{\int_\Omega (u_i^n)^p dx}$$

if $\int_\Omega (u_i^n)^p dx > 0$. Otherwise, $c_i^n = 0$. It is easy to get that

$$0 \le c_i^n \le \|I\|_{L^\infty(\Omega)}.$$

By the boundedness of sequence $\{c_i^n\}$, we can abstract a subsequence also denoted by $\{c_i^n\}$ and a constant c_i^* such that

$$c_i^n \to c_i^* \quad \text{uniformly.}$$

Finally, since $u_i^n \to u_i^*$, a.e. $x \in \Omega$ and $c_i^n \to c_i^*$, Fatou's lemma gives

$$\int_\Omega (I - c_i^*)^2 (u_i^*)^p dx \le \liminf_{n\to\infty} \int_\Omega (I - c_i^n)^2 (u_i^n)^p dx. \tag{3.7}$$

Combining inequalities (3.6) and (3.7) for all i, on a suitable subsequence, we have established that

$$E(U^*, c^*) \le \liminf_{n\to\infty} E(U^n, c^n) = \inf E(U, c), \tag{3.8}$$

and hence (U^*, c^*) must be a minimizer. This completes the proof. ∎

Note that the above energy functional $E(U, c)$ is symmetric with respect to the arguments (U, c); hence we can easily deduce that the minimizer of $E(U, c)$ is symmetric. That is, if (U^*, c^*) is a minimizer, then (U_γ^*, c_γ^*) is also a minimizer, where γ denotes a permutation of $\{1, \ldots, N\}$.

The existence of minimizers of the energy holds for some more general error functions such as the error functions in the region competition model which follow Gaussian distributions. It can be shown using the same arguments as in Theorem 3.1.

4. Alternative minimization. For efficiency in minimizing energy (3.3), we choose to follow [3, 17, 11] and make use of Chambolle's fast dual projection algorithm [8]. To this end, we add auxiliary variables $V = (v_1, \ldots, v_N)$ and approximate E in (3.3) by

$$E_r(U, V, \alpha) = \sum_{i=1}^N \left\{ \frac{\lambda}{p} \int_\Omega r_i(I, \alpha_i) u_i^p dx + \int_\Omega |\nabla v_i| dx + \frac{1}{2\theta} \int_\Omega (v_i - u_i)^2 dx \right\}, \tag{4.1}$$

where θ is chosen small enough so that u_i and v_i are almost identical with respect to the L^2 norm. We use an alternative minimization method to minimize energy E_r.

4.1. Solving region parameters α. With U and V fixed, we need to minimize

$$E_1(\alpha) = \sum_{i=1}^{N} \int_\Omega r_i(I, \alpha_i) u_i^p dx$$

with respect to α. The solution of region parameters depends on the error function $r_i(I, \alpha_i)$. Here we consider the Chan–Vese error function and its local version.

Let $r_i(I, \alpha_i) = (I - c_i)^2$; then $\alpha = c$. Taking the derivative of $E_1(\alpha)$ with respect to c_i and setting the result to zero, we obtain the closed form solution

$$c_i = \frac{\int_\Omega I(x) u_i^p(x) dx}{\int_\Omega u_i^p(x) dx}. \tag{4.2}$$

The Chan–Vese model assumes that the image can be approximated by piecewise constant functions. In practice, images that could be accurately approximated by piecewise constant functions are rarely encountered. In some applications, this hypothesis holds locally. To that end, we extend the model to cases of local errors following [14, 17]. To realize localization, we introduce a symmetric Gaussian kernel function $\omega : \Omega \to \mathbb{R}$ satisfying

$$\int_\Omega \omega(x) dx = 1, \qquad \omega(-x) = \omega(x).$$

Then the local error function at $x \in \Omega$ is

$$r_i(I, \alpha_i)(x) = \int_\Omega (I(x) - s_i(y))^2 \omega(x - y) dy, \tag{4.3}$$

where the region parameter $\alpha_i = s_i$ is a function. Taking the derivative of $E_1(\alpha)$ with respect to the parameter s_i, we obtain

$$\int_\Omega (I(x) - s_i(y)) \omega(x - y) u_i^p(x) dx = 0.$$

Then we derive

$$s_i(y) = \frac{\int_\Omega I(x) \omega(x - y) u_i^p(x) dx}{\int_\Omega \omega(x - y) u_i^p(x) dx},$$

which can be simplified by the convolution operator as

$$s_i = \frac{\omega * (I u_i^p)}{\omega * u_i^p}. \tag{4.4}$$

4.2. Solving auxiliary variables V. Fixing U and α, we solve v_i by minimizing

$$\int_\Omega |\nabla v_i| dx + \frac{1}{2\theta} \int_\Omega (v_i - u_i)^2 dx.$$

This problem can be efficiently solved by the fast dual projection algorithm. The solution is given by

$$v_i = u_i - \theta \operatorname{div} p_i^*, \quad i = 1, \ldots, N, \tag{4.5}$$

where the vector p_i^* can be solved by the fixed point method: Initialize $p_i^0 = 0$ and iterate

$$p_i^{n+1} = \frac{p_i^n + \tau \nabla (\operatorname{div} p_i^n - u_i/\theta)}{1 + \tau |\nabla (\operatorname{div} p_i^n - u_i/\theta)|} \tag{4.6}$$

with $\tau \le 1/8$ to ensure convergence. See [8] for more details.

4.3. Solving membership functions U. Fixing V and α, using the simplified notation $r_i = r_i(I, \alpha_i)$, we consider the optimization problem

$$\min E_2(U) = \frac{\lambda}{p} \sum_{i=1}^{N} \int_\Omega r_i u_i^p dx + \frac{1}{2\theta} \sum_{i=1}^{N} \int_\Omega (v_i - u_i)^2 dx \tag{4.7}$$

subject to

$$\text{(i)} \quad \sum_{i=1}^{N} u_i(x) - 1 = 0,$$
$$\text{(ii)} \quad 0 \le u_i(x) \le 1 \quad \text{for } i = 1, \dots, N.$$

We give three methods for solving this optimization problem.

4.3.1. Method I. We set $p = 1$ and relax constraint (i) by adding a penalization term and minimizing the approximate energy

$$E_{2a}(U) = \lambda \sum_{i=1}^{N} \int_\Omega r_i u_i dx + \frac{1}{2\theta} \sum_{i=1}^{N} \int_\Omega (v_i - u_i)^2 dx + \frac{\nu}{2} \int_\Omega \left(\sum_{i=1}^{N} u_i - 1 \right)^2 dx \tag{4.8}$$

subject to

$$0 \le u_i(x) \le 1 \quad \text{for } i = 1, \dots, N,$$

where ν, a given large positive constant, is a penalization parameter.

Since the objective function is quadratic and positive and the feasible region is convex, there exists a unique global minimizer of (4.8). However, the exact solution cannot be written easily. In order to give an approximate numerical solution, we do not consider the constraint requirement at first. Then the optimal condition is

$$\frac{\partial E_{2a}(U)}{\partial u_i} = \lambda r_i + \frac{1}{\theta}(u_i - v_i) + \nu \left(\sum_{i=1}^{N} u_i - 1 \right) = 0.$$

It is easy to check that the solution is

$$u_i = v_i - \lambda \theta r_i - \frac{\nu\theta \left(\sum_{j=1}^{N} (v_j - \lambda\theta r_j) - 1 \right)}{1 + N\nu\theta}.$$

Next we apply the constraint by projecting u_i onto [0,1]; that is,

$$\hat{u}_i := \min\{\max\{u_i, 0\}, 1\}. \tag{4.9}$$

Here $\hat{u}_i$ gives an approximate numerical solution to (4.8). We find in the experimental results that such approximate numerical solutions can achieve good segmentation results.

4.3.2. Method II. We set $p = 1$ and relax constraint (i) by letting

$$u_N = 1 - \sum_{i=1}^{N-1} u_i$$

and getting rid of the constraint $0 \le u_N \le 1$. Using this formula of u_N in energy (4.7), we then need to minimize the approximate energy

$$E_{2b}(\bar{U}) = \lambda \sum_{i=1}^{N-1} \int_\Omega (r_i - r_N)\, u_i dx + \frac{1}{2\theta} \sum_{i=1}^{N-1} \int_\Omega (v_i - u_i)^2 dx \tag{4.10}$$

subject to

$$0 \le u_i(x) \le 1 \quad \text{for } i = 1, \dots, N-1,$$

where $\bar{U} = (u_1, \dots, u_{N-1})$. There exists a unique global minimizer by the convexity of the problem. In this case, we can obtain the exact solution of the approximate problem by using KKT conditions.

Assume that $\bar{U}^* = (u_1^*, \dots, u_{N-1}^*)$ is the unique solution of (4.10). Then the following KKT conditions are both necessary and sufficient: Suppose that $\tilde{U}^*$ is the global minimizer of (4.10); then

(a) $u_i^*(x) \ge 0,\ 1 - u_i^*(x) \ge 0$;

(b) there exist Lagrange multipliers $\beta_i^*(x)$ and $\gamma_i^*(x)$ for each point $x \in \Omega$ such that

$$\frac{\partial E_{2a}(U)}{\partial u_i^*(x)} = \lambda(r_i(x) - r_N(x)) + \frac{1}{\theta}(u_i^*(x) - v_i(x)) = \beta_i^*(x) - \gamma_i^*(x);$$

(c) $\beta_i^*(x) u_i^*(x) = 0,\ \gamma_i^*(x)(1 - u_i^*(x)) = 0$;

(d) $\beta_i^*(x) \ge 0,\ \gamma_i^*(x) \ge 0$

for $i = 1, \dots, N-1$.

First we assume that $\tilde{U} = (\tilde{u}_1, \dots, \tilde{u}_{N-1})$ satisfies

$$\lambda(r_i(x) - r_N(x)) + \frac{1}{\theta}(\tilde{u}_i(x) - v_i(x)) = 0.$$

The solution is

$$\tilde{u}_i = v_i - \lambda\theta(r_i - r_N).$$

Then we construct $\hat{u}_i$ by projecting $\tilde{u}_i$ onto [0,1]; that is,

$$\hat{u}_i := \min\{\max\{\tilde{u}_i, 0\}, 1\}. \tag{4.11}$$

Let $\hat{\eta}_i(x) = \lambda(r_i(x) - r_N^{\alpha_N}(x)) + \frac{1}{\theta}(\hat{u}_i(x) - v_i(x))$, and let $\tilde{\eta}_i(x) = \lambda(r_i(x) - r_N^{\alpha_N}(x)) + \frac{1}{\theta}(\tilde{u}_i(x) - v_i(x)) = 0$. For each $x \in \Omega$, we choose $\hat{\beta}_i(x)$ and $\hat{\gamma}_i(x)$ as follows:

If $\hat{u}_i(x) \in (0,1)$, then $\tilde{u}_i(x) \in (0,1)$ and $\tilde{u}_i(x) = \hat{u}_i(x)$; hence $\hat{\eta}_i(x) = \tilde{\eta}_i(x) = 0$. Set $\hat{\beta}_i(x) = 0$ and $\hat{\gamma}_i(x) = 0$.

If $\hat{u}_i(x) = 0$, then $\tilde{u}_i(x) \le 0$ and $\hat{u}_i(x) \ge \tilde{u}_i(x)$; hence $\hat{\eta}_i(x) \ge \tilde{\eta}_i(x) = 0$. Set $\hat{\beta}_i(x) = \hat{\eta}_i(x)$ and $\hat{\gamma}_i(x) = 0$.

If $\hat{u}_i(x) = 1$, then $\tilde{u}_i(x) \geq 1$ and $\hat{u}_i(x) \leq \tilde{u}_i(x)$; hence $\hat{\eta}_i(x) \leq \tilde{\eta}_i(x) = 0$. Set $\hat{\beta}_i(x) = 0$ and $\hat{\gamma}_i(x) = -\hat{\eta}_i(x)$.

Then it is easy to verify that $\{\hat{u}_i, \hat{\beta}_i, \hat{\gamma}_i\}$ satisfies KKT conditions (a)–(d). Therefore $\hat{U}$ is a minimizer of problem (4.10), and by uniqueness $U^* = \hat{U}$.

Finally, we conclude that in this method the approximate numerical solution for the membership function is given by (4.11).

4.3.3. Method III. Assume that $p = 2$. We consider the optimization problem

$$\min E_{2c}(U) = \frac{\lambda}{2}\sum_{i=1}^{N}\int_{\Omega} r_i u_i^2 dx + \frac{1}{2\theta}\sum_{i=1}^{N}\int_{\Omega}(v_i - u_i)^2 dx \tag{4.12}$$

subject to

$$\text{(i)} \quad \sum_{i=1}^{N} u_i(x) - 1 = 0,$$
$$\text{(ii)} \quad 0 \leq u_i(x) \leq 1 \quad \text{for } i = 1, \ldots, N.$$

Though there exists a unique global minimizer of the problem (4.12), it is also hard to get the exact solution. Hence we turn to finding the approximate solution. As in Method I, we do not consider the inequality constraint requirement at first. By adding pointwise Lagrange multipliers $\delta(x)$ to handle the equality constraints, we need to minimize

$$\frac{\lambda}{2}\sum_{i=1}^{N}\int_{\Omega} r_i u_i^2 dx + \frac{1}{2\theta}\sum_{i=1}^{N}\int_{\Omega}(v_i - u_i)^2 dx + \int_{\Omega}\delta(x)\left(\sum_{i=1}^{N} u_i - 1\right)dx.$$

The optimal condition is

$$\lambda r_i(x)u_i(x) + \frac{1}{\theta}(u_i(x) - v_i(x)) + \delta(x) = 0.$$

Then the closed form solution of u_i is given by

$$u_i = \frac{v_i - \theta\delta}{1 + \lambda\theta r_i}.$$

By applying the constraint $\sum_{i=1}^{N} u_i = 1$ to the obtained solution, we have

$$\sum_{i=1}^{N}\frac{v_i - \theta\delta}{1 + \lambda\theta r_i} = 1;$$

then

$$\delta = \frac{\sum_{i=1}^{N}\frac{v_i}{1+\lambda\theta r_i} - 1}{\theta\sum_{i=1}^{N}\frac{1}{1+\lambda\theta r_i}}. \tag{4.13}$$

Substituting δ into the formula of u_i gives

$$u_i = \frac{v_i}{1 + \lambda\theta r_i} - \frac{\sum_{j=1}^{N}\frac{v_j}{1+\lambda\theta r_j} - 1}{\sum_{j=1}^{N}\frac{1+\lambda\theta r_i}{1+\lambda\theta r_j}}.$$

Next we can apply the inequality constraints by projecting u_i onto [0,1]:

$$\hat{u}_i := \min\{\max\{u_i, 0\}, 1\}. \tag{4.14}$$

Here $\hat{u}_i$ gives an approximate numerical solution for the membership function. We also find in the experimental results that such approximate numerical solutions can achieve good segmentation results.

Note that besides the above settings, we can set $p = 2$ in Methods I and II, and set $p = 1$ in Method III. Their corresponding solutions can be obtained by using similar techniques; thus the solution procedure is omitted. For $p \neq 1, 2$, the closed form solution cannot be obtained in general. Numerical optimization procedures must be employed in order to obtain solutions. On the other hand, in the special case of $N = 2$, our Method II is equal to the algorithm in [17]; see (2.6). Methods I and III are new even for two-phase image segmentation.

4.4. Algorithm details. We choose the Chan–Vese error function as an example to describe the algorithm of minimizing E_r. The algorithm can be summarized in the following steps.

- Initialization: Initialize the membership functions u_i by random matrices where each entry follows a uniform distribution in $[0, 1]$, and then normalize them such that membership constraints (i) and (ii) are both satisfied. Set $v_i^0 = u_i^0$, $c_i^0 = 0$.
- Iteration: Update c_i^k by formula (4.2); update v_i^k by formula (4.5); update u_i^k by formula (4.9) in Method I, (4.11) in Method II, or (4.14) in Method III.
- Termination criterion:
$$\|c^k - c^{k-1}\| \leq \epsilon,$$
where $c^k = (c_1^k, \ldots, c_N^k)$ is the vector of centers, $\|\cdot\|$ denotes the Euclidean distance, and ϵ is a small positive number defined by the user.

We remark that, in the above iterations, when we update v_i^k by formula (4.5) and get the p_i^* in (4.5), we need only iterate (4.6) one time with initial value p_i^0 equal to the p_i^* value in the last loop of the alternative minimization. It is well known that the original Chambolle dual projection algorithm sets $p_i^0 = 0$. Our initialization makes use of the information of p_i^* obtained in the last loop in the alternative minimization process and is more efficient. In our algorithm, the solution of membership functions and region parameters is given by a closed form solution, while the auxiliary variables can be solved by one iteration of Chambolle's projection so that the algorithm is very efficient. In contrast, the use of level set functions for the Chan–Vese model requires solving by the gradient descent method with a small time step, and the convergence of the gradient descent method is slow.

4.5. Convergence of the algorithm. For simplicity, we choose the Chan–Vese error function. By running the algorithm, we get sequences

$$(c_i^0, v_i^0, u_i^0, c_i^1, v_i^1, u_i^1, \ldots, c_i^k, v_i^k, u_i^k, \ldots). \tag{4.15}$$

We introduce the simplified notation c^k, V^k, and U^k to denote the sequences about c_i^k, v_i^k, and u_i^k for all $i = 1, \ldots, N$. We show here that our algorithm gives a coordinatewise minimum of the constrained problem (4.1) in the strong assumption that Methods I–III provide the exact solution which has not been shown.

Theorem 4.1. *The sequence* (U^k, V^k, c^k) *given by* (4.15) *converges to a coordinatewise minimum of* E_r *on* $X = BV_{[0,1]}(\Omega)^N \times BV(\Omega)^N \times \mathbb{R}^N$.

Proof. As we solve alternative minimization problems, we have

$$\begin{aligned} E_r(U^{k+1}, V^{k+1}, c^{k+1}) &\le E_r(U^k, V^{k+1}, c^{k+1}) \\ &\le E_r(U^k, V^k, c^{k+1}) \le E_r(U^k, V^k, c^k). \end{aligned} \tag{4.16}$$

In particular, the sequence $E_r(U^k, V^k, c^k)$ is nonincreasing and bounded by zero. Thus it converges in $\mathbb{R}$. Denote the limit by m, that is,

$$m = \lim_{k\to\infty} E_r(U^k, V^k, c^k).$$

As in the proof of Theorem 3.1, we can prove that E_r is coercive. As the sequence $E_r(U^k, V^k, c^k)$ converges, we deduce that the sequence (U^k, V^k, c^k) is bounded in X. Hence, we can extract a subsequence $(U^{k_n}, V^{k_n}, c^{k_n})$ which converges to $(\hat{U}, \hat{V}, \hat{c}) \in X$ as $k_n \to \infty$; that is,

$$(U^{k_n}, V^{k_n}, c^{k_n}) \to (\hat{U}, \hat{V}, \hat{c}). \tag{4.17}$$

Moreover, from (4.16), for all $k_n \in \mathbb{N}$ and all $c \in \mathbb{R}^n$

$$E_r(U^{k_n}, V^{k_n}, c^{k_n+1}) \le E_r(U^{k_n}, V^{k_n}, c), \tag{4.18}$$

for all $k_n \in \mathbb{N}$ and all $V \in BV(\Omega)^N$

$$E_r(U^{k_n}, V^{k_n+1}, c^{k_n+1}) \le E_r(U^{k_n}, V, c^{k_n+1}), \tag{4.19}$$

and for all $k_n \in \mathbb{N}$ and $U \in BV_{[0,1]}(\Omega)^N$

$$E_r(U^{k_n}, V^{k_n}, c^{k_n}) \le E_r(U, V^{k_n}, c^{k_n}). \tag{4.20}$$

By (4.2), the closed form solution of $c_i^{k_n+1}$ is

$$c_i^{k_n+1} = \frac{\int_\Omega I(u_i^{k_n})^p dx}{\int_\Omega (u_i^{k_n})^p dx}. \tag{4.21}$$

By passing to the limit in (4.21) as $k_n \to +\infty$, we get

$$c^{k_n+1} \to \frac{\int_\Omega I\hat{u}_i dx}{\int_\Omega \hat{u}_i dx} = \hat{c}. \tag{4.22}$$

Meanwhile, by formula (4.5), we have

$$v_i^{k_n+1} = u_i^{k_n} - \theta \operatorname{div} p_i^*(u_i^{k_n}), \tag{4.23}$$

where $p_i^*(u_i^{k_n})$ means p_i^* is dependent on $u_i^{k_n}$. By passing to the limit in (4.23) as $k_n \to +\infty$, we get

$$v_i^{k_n+1} \to \hat{u}_i - \theta \operatorname{div} p_i^*(\hat{u}_i) = \hat{v}_i. \tag{4.24}$$

By (4.17), (4.22), and (4.24), we can pass to the limit in (4.18), (4.19), and (4.20), and therefore we have for all $c \in \mathbb{R}^n$

$$E_r(\hat{U}, \hat{V}, \hat{c}) \leq E_r(\hat{U}, \hat{V}, c), \tag{4.25}$$

for all $V \in BV(\Omega)^N$

$$E_r(\hat{U}, \hat{V}, \hat{c}) \leq E_r(\hat{U}, V, \hat{c}), \tag{4.26}$$

and for all $U \in BV_{[0,1]}(\Omega)^N$

$$E_r(\hat{U}, \hat{V}, \hat{c}) \leq E_r(U, \hat{V}, \hat{c}). \tag{4.27}$$

Inequalities (4.25), (4.26), and (4.27) can be rewritten, respectively, as

$$E_r(\hat{U}, \hat{V}, \hat{c}) = \inf_c E_r(\hat{U}, \hat{V}, c), \tag{4.28}$$

$$E_r(\hat{U}, \hat{V}, \hat{c}) = \inf_V E_r(\hat{U}, V, \hat{c}), \tag{4.29}$$

$$E_r(\hat{U}, \hat{V}, \hat{c}) = \inf_U E_r(U, \hat{V}, \hat{c}). \tag{4.30}$$

Then we have for $i = 1, \ldots, N$

$$0 \in \frac{\partial E_r}{\partial c_i}(\hat{U}, \hat{V}, \hat{c}), \qquad 0 \in \frac{\partial E_r}{\partial v_i}(\hat{U}, \hat{V}, \hat{c}), \qquad 0 \in \frac{\partial E_r}{\partial u_i}(\hat{U}, \hat{V}, \hat{c}).$$

Finally we can conclude that $(\hat{U}, \hat{V}, \hat{c})$ is a coordinatewise minimum with energy $E_r(\hat{U}, \hat{V}, \hat{c}) = m$. ∎

Note that the proposed algorithm may not converge to the global minimum since the energy E_r is not globally convex.

5. Extension to vector-valued images. It is straightforward to extend the algorithm to vector-valued images. Assume that $I : \Omega \to \mathbb{R}^m$ is the vector-valued image; then the Chan–Vese error of the jth channel is defined by

$$r_{i,j}(I_j, c_{i,j}) = (I_j - c_{i,j})^2.$$

The ith error function is then the average of the errors of the m channels, that is,

$$r_i(I, c_i) = \sum_{j=1}^{m} r_{i,j}(I_j, c_{i,j}),$$

where $c_i = (c_{i,1}, \ldots, c_{i,N})$ is a vector. It is easy to derive the formula of $c_{i,j}$:

$$c_{i,j} = \frac{\int_\Omega I_j(x) u_i^p(x) dx}{\int_\Omega u_i^p(x) dx}.$$

Then we can get that the numerical algorithm for vector-valued images just follows the algorithm in section 4 for grayscale images by using new formulas for c_i and r_i, and thus it is omitted.

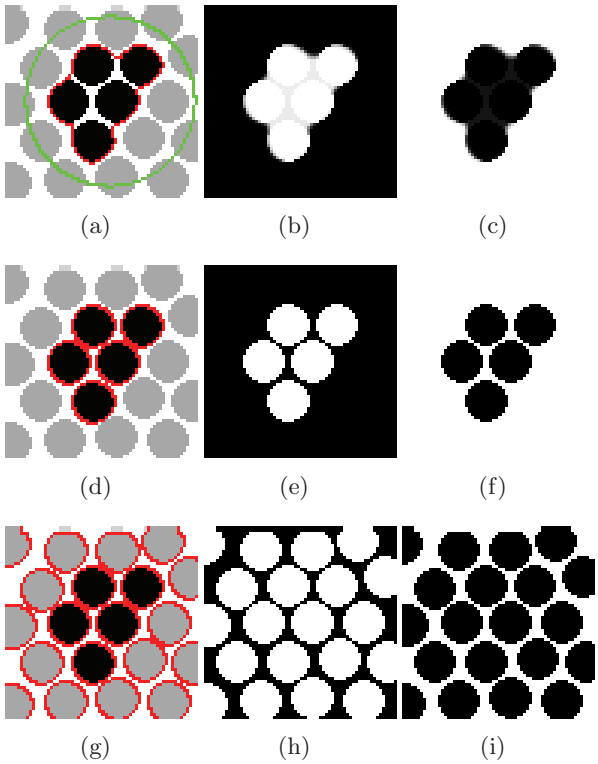

Figure 1. *Two-phase segmentation. The test image is of size* 64×64. (a) *The contour of the initial guess (green) and the contour of the final segmentation (red) with* $\lambda = 0.0002$; (b)–(c) *the membership functions in* (a); (d) *the segmentation result with* $\lambda = 0.01$; (e)–(f) *the membership functions in* (d); (g) *the segmentation result with* $\lambda = 10$; *and* (h)–(i) *the membership functions in* (g).

6. Experimental results. We test our algorithm on synthetic images and real (grayscale and color) images. We test Methods I, II, and III for solving membership functions. In all the experiments, we choose the Chan–Vese error function in section 3 or the local error function in (4.3). Some parameters are fixed as follows: $\theta = 0.1$, $\nu = 1000$, $\epsilon = 10^{-4}$. The parameter λ is required to be tuned for each image. We initialize the membership functions u_i by random matrices where each entry follows a uniform distribution in $[0, 1]$, and then we normalize them such that the membership constraints are satisfied. We also consider a special initialization in two-phase image segmentation. We draw a circle on the image and set the membership function $u_1^0 = 1$ inside the circle and $u_1^0 = 0$ outside. For u_2^0, we set $u_2^0 = 1 - u_1^0$. The circle is shown in green. In all the experiments, the final segmentation results are obtained by checking the class at each pixel where the corresponding membership function value is the largest. The experiments are performed using Windows XP and MATLAB v7.4 with Intel Core 2 Duo CPU at 1.66 GHz and 2GB memory.

6.1. Two-phase segmentation. Two-phase segmentation results for grayscale images with the Chan–Vese error function are reported in Figures 1–3. It is shown that our fuzzy model retains the advantages of the level set method based on the Chan–Vese model. Indeed, we can segment objects whose boundaries cannot be defined or are badly defined through their

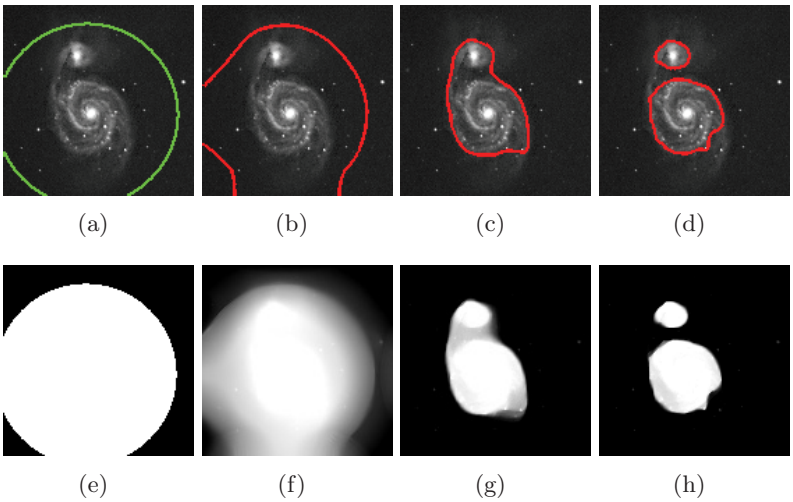

Figure 2. *Two-phase segmentation. The test image is of size* 137×137*, and* $\lambda = 0.0001$ *is set.* (a) *The contour of the initial guess (green);* (b)–(c) *the intermediate segmentations (red);* (d) *the final segmentation (red);* (e) *the initial membership functions;* (f)–(g) *the intermediate membership functions; and* (h) *the final membership.*

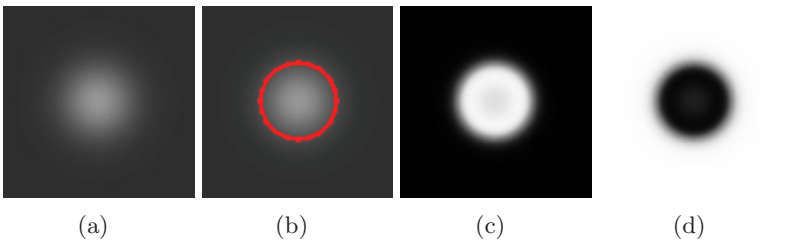

Figure 3. *Two-phase segmentation. The test image is of size* 100×100*, and* $\lambda = 0.1$ *is set.* (b) *The segmentation result, and* (c)–(d) *the membership functions.*

gradients. This includes, for example, smeared boundaries (see Figures 2(d) and 3(b)) and cognitive contours (boundaries of larger objects defined by grouping smaller ones; see Figure 1(a)).

We use Method I to solve membership functions as shown in Figure 1. In the procedure of tuning the parameter λ, we observe that the value of λ greatly affects the segmentation result. For $\lambda = 0.0002$ in Figure 1(a), the initial and the final segmentations are marked with green and red contours, respectively. The result shows that our algorithm can get cognitive contours. The two corresponding membership functions are displayed in Figures 1(b) and 1(c). Figures 1(d) and 1(g) give the segmentation results for $\lambda = 0.01$ and $\lambda = 10$, respectively. Their corresponding membership functions are also shown in Figures 1(e)–1(f) and Figures 1(h)–1(i), respectively. We note that random initialization is used to obtain the results in Figures 1(d) and 1(g). We also find that when λ is in the range of $[0.0005, 1]$, we get the same segmentation result as shown in Figure 1(d). When $\lambda \geq 10$, we obtain almost the same segmentation result as shown in Figure 1(g).

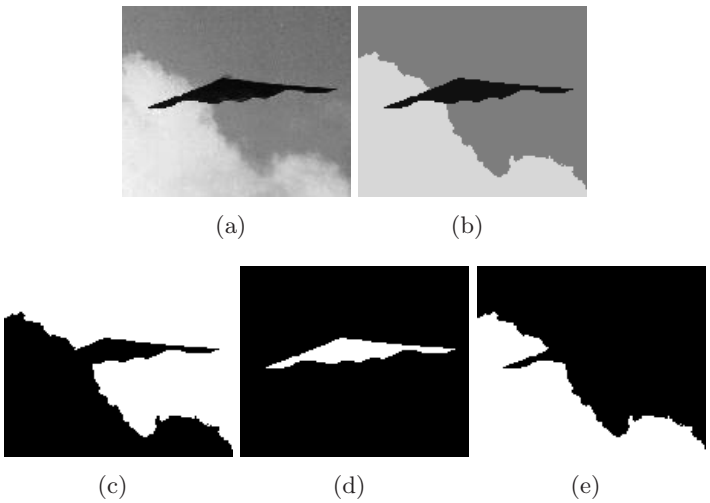

Figure 4. *Three-phase segmentation using Method* II *with* $\lambda = 0.2$. (a) *The test image is of size* 150×125; (b) *the piecewise constant image; and* (c)–(e) *membership functions* u_1, u_2, u_3.

Next we use Method I to perform image segmentation for the galaxy image shown in Figure 2. In the figure, we show the intermediate and final segmentation results. We find that the algorithm can obtain the smeared contours of the galaxy.

In Figure 3, we also use Method I to perform image segmentation for a case of smooth boundary detection. In this example, we consider random initialization of membership functions. When λ is set to 0.1, the segmentation result is shown in Figure 3(b), and the corresponding membership functions are shown in Figures 3(c)–3(d). Indeed, for quite a large range of λ (0.001–1000), we obtain the same segmentation result as shown in Figure 3(b).

We remark that the other two methods (Methods II and III) provide similar results in Figures 1, 2, and 3.

6.2. Multiphase segmentation. In this subsection, we test the proposed methods for multiphase image segmentation of grayscale and color images. In these examples, we use the Chan–Vese error function.

In the first example, we show the three-phase segmentation results using Method II. Figure 4(b) shows the piecewise constant approximation (three constants) of the test image given in Figure 4(a). The corresponding membership functions are displayed in Figures 4(c)–4(e), respectively.

In the second example, we show the five-phase segmentation results using Method III. The test image is contaminated by zero mean Gaussian noise with standard deviation 10; see Figure 5(a). Figure 5(b) shows the piecewise constant approximation (five constants) of the test image. The corresponding membership functions are displayed in Figures 5(c)–5(g), respectively.

In the third example, we show the three-phase color segmentation results using Method I. The test image in Figure 6(a) contains some textures in the background. Figure 6(b) shows the piecewise constant approximation (three-color vectors) of the test image. The corresponding membership functions are displayed in Figures 6(c)–6(e), respectively.

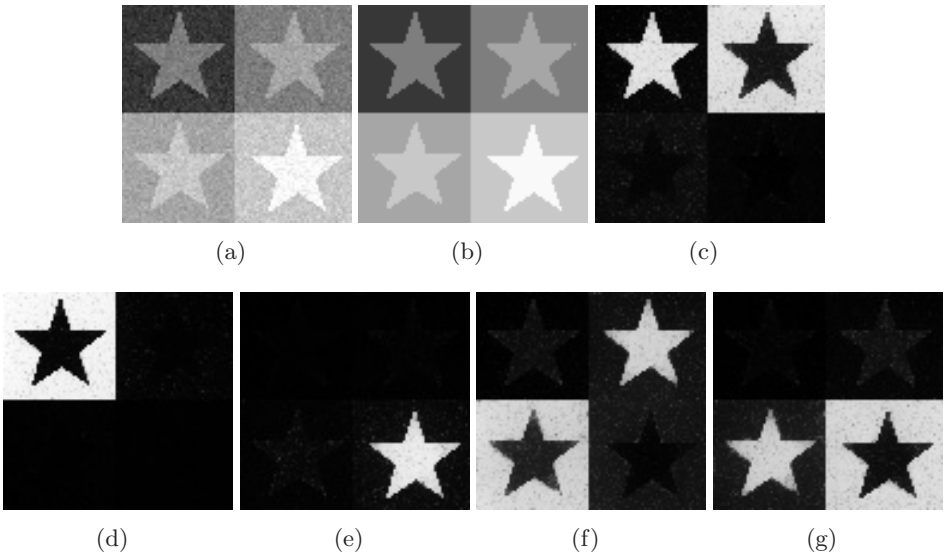

Figure 5. *Five-phase segmentation using Method* III *with* $\lambda = 0.005$. (a) *The test image is of size* 96×91*, and Gaussian noise with zero mean and standard deviation* 10 *is added;* (b) *the piecewise constant image; and* (c)–(g) *membership functions* u_1, u_2, u_3, u_4, u_5.

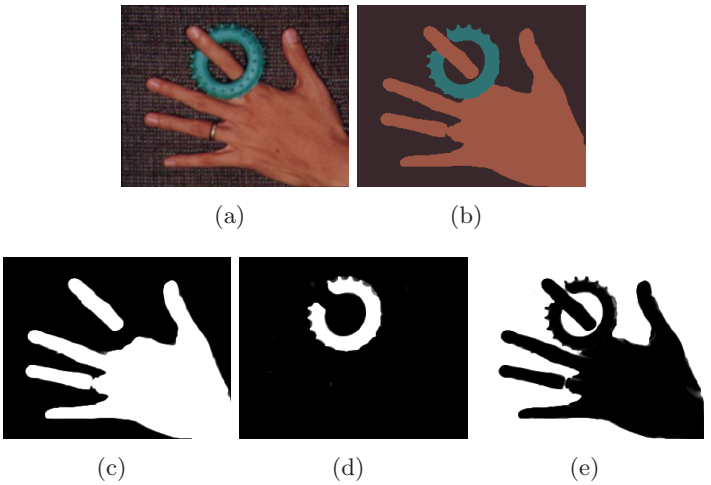

Figure 6. *Three-phase color segmentation using Method* I *with* $\lambda = 0.01$. (a) *The test image is of size* 303×241; (b) *the piecewise constant color image; and* (c)–(e) *the membership functions* u_1, u_2, u_3.

In the fourth example, we show the six-phase color segmentation results using Method III. The test image is a synthetic image, and zero mean Gaussian noise with standard deviation 50 is added; see Figure 7(a). Figure 7(b) shows the piecewise constant approximation (six-color vectors) of the test image. The corresponding membership functions are displayed in Figures 7(c)–7(h), respectively.

Because noise is added in Figures 5(a) and 7(a), some membership functions values are not close to 0 or 1. The final segmentation results are given by taking the maximal among membership function values, and the results are quite good.

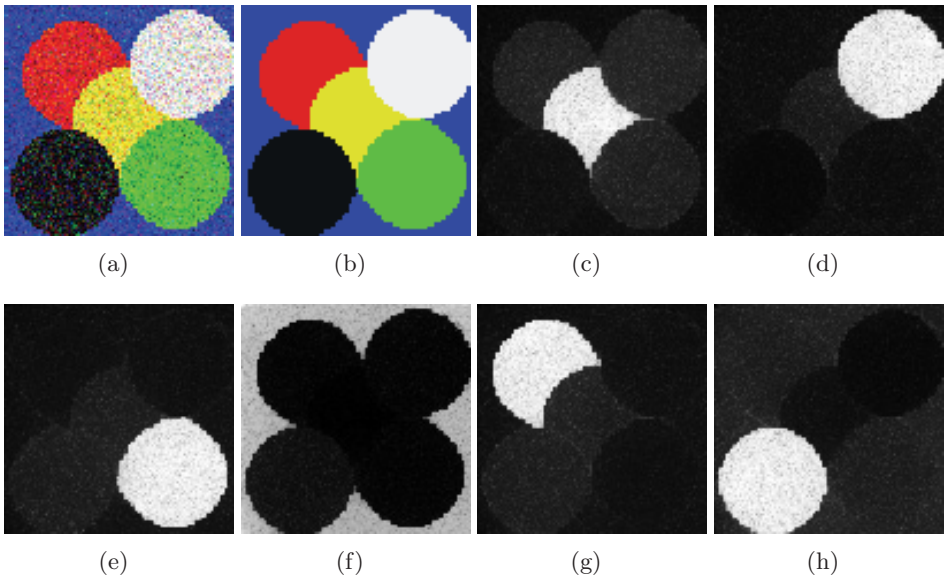

Figure 7. *Six-phase color segmentation using Method* III *with* $\lambda = 0.0005$. (a) *The test image is of size* 100×100 *and is contaminated by Gaussian zero mean noise with standard deviation* 50; (b) *the piecewise constant color image; and* (c)–(h) *the membership functions* $u_1, u_2, u_3, u_4, u_5, u_6$.

6.3. Comparison with other segmentation methods. In this subsection, we compare the proposed method with other segmentation methods.

In the first example, we consider the comparison of two-phase segmentation with different methods. Figure 8(a) is a test vessel image with inhomogeneous intensity. With the Chan–Vese error function and Method I, our algorithm fails to delineate the boundary of the vessel; see Figure 8(c). The level set based Chan–Vese model also fails; see Figure 4(d). In contrast, with local error function (4.3) and Method I, our algorithm can give a more satisfactory result in Figure 8(b). Here we use the same initialization to obtain the segmentation results in Figures 8(b)–8(d). The corresponding membership function along time in the segmentation process is displayed in Figures 8(e)–8(h). We find in these figures that membership function values are not close to 0 or 1 at some boundary pixels. We remark that with the local error function, Methods II and III also work and the segmentation results are similar to those in Figure 8(b).

In the second example, we compare the proposed algorithm with the method in [16] for four-phase image segmentation. Figure 9(a) is the original piecewise constant image, and Figure 9(b) is the noisy test image. Figure 9(c) shows the piecewise constant approximation using the proposed algorithm (Method III). Figures 9(d)–9(f) show the results of the method in [16] with different initializations. We employ the method in [16] with the parameters $dt = 0.0004$, $\beta = 1.5$, and $r = 2.5$. In order to quantify the segmentation results, we use segmentation accuracy, which is defined as the ratio of the number of rightly classified pixels to the total number of pixels. The experiment results show that the segmentation accuracy and computational time of the method in [16] are quite sensitive to the initialization of initial piecewise constants. With good initial piecewise constants, the method is very fast

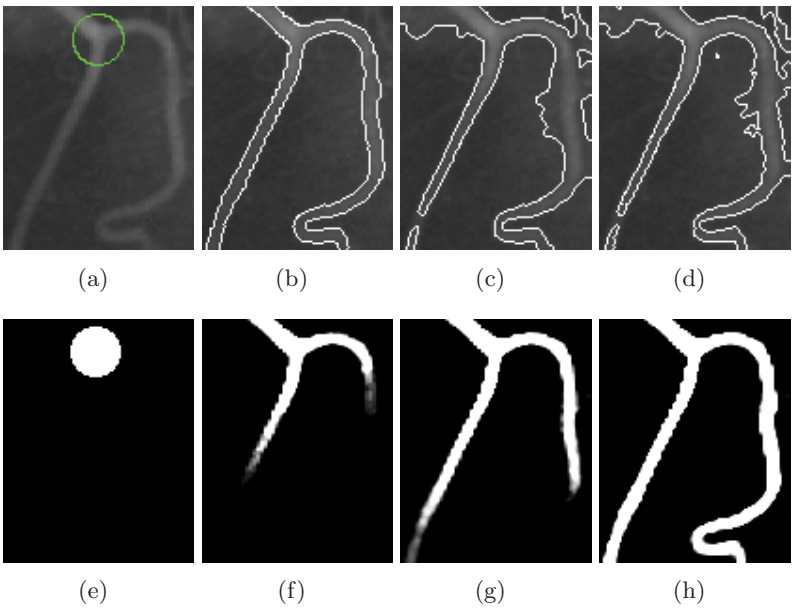

Figure 8. *Comparison of two-phase segmentation.* (a) *The test image is of size* 102×130 *with the initial guess (the green contour);* (b) *the segmentation result using Method* I *and local error function* (4.3) *with* $\lambda = 0.01$; (c) *the segmentation result using Method* I *and the Chan–Vese error function with* $\lambda = 0.01$; (d) *the segmentation result using the level set based Chan–Vese model; and* (e)–(h) *the membership function* u_1 *along time in the segmentation process with Method* I *using the local error function.*

and the image can be segmented correctly. However, when the initial piecewise constants are far from the suitable values, the computational time increases and the segmentation accuracy decreases. In contrast, our algorithm can give an accurate segmentation using random membership functions in Figure 9. These results show that our algorithm is less sensitive to initialization.

In the third example, we compare our algorithm (Method III) with the level set method based Chan–Vese model for four-phase segmentation. The piecewise constant segmentation result of our algorithm is shown in Figure 10(b), and the membership functions are shown in Figures 10(c)–10(f). For the four-phase Chan–Vese model, two level sets, ϕ_1, ϕ_2, are needed. Figures 10(g) and 10(h) display the initial and the final zero level sets. Figure 10(i) shows the piecewise constant image given by formula $\sum_{i=1}^{4} c_i \chi_{\Omega_i}$, where $\chi_{\Omega_i}, i = 1 : 4$, are the characteristic functions of the following four regions: $\Omega_1 = \{x | \phi_1(x) \geq 0, \phi_2(x) \geq 0\}$, $\Omega_2 = \{x | \phi_1(x) \geq 0, \phi_2(x) < 0\}$, $\Omega_3 = \{x | \phi_1(x) < 0, \phi_2(x) \geq 0\}$, and $\Omega_4 = \{x | \phi_1(x) < 0, \phi_2(x) < 0\}$. It is obvious that our segmentation result in Figure 10(b) is more accurate than the result in Figure 10(i). According to Figure 10(a), we find that the four regions (sky, yellow flowers, red flowers, and stem) do not have constant intensity in the corresponding color. Therefore our segmentation results give some membership function values that are not close to 0 or 1; see Figures 10(c)–10(f).

We also compare the computational times of the two methods. Our algorithm converges at 52 iterations consuming 7.1 seconds, while the Chan–Vese model converges at 100 iterations consuming 14.5 seconds. Note that, in our implementation of the Chan–Vese model, in order

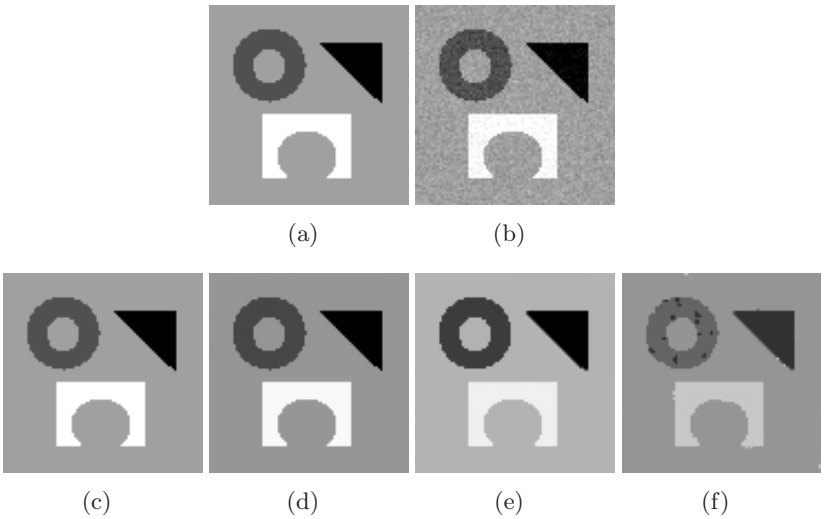

Figure 9. *Comparison of four-phase segmentation.* (a) *The original piecewise constant image of size* 90×90; (b) *the image contaminated by Gaussian noise with zero mean and standard deviation* 10; (c) *the piecewise constant segmentation by Method* III *with* $\lambda = 0.05$ *(computational time* $= 0.9$ *seconds, number of iterations* $= 42$*, segmentation accuracy* $= 100\%$*);* (d) *the piecewise constant segmentation by the method in* [16] *(initial* $c = [0, 70, 150, 250]$*, computational time* $= 1$ *second, segmentation accuracy* $= 100\%$*);* (e) *the piecewise constant segmentation by the method in* [16] *(initial* $c = [0, 60, 180, 240]$*, computational time* $= 63$ *seconds, segmentation accuracy* $= 99.67\%$*); and* (f) *the piecewise constant segmentation by the method in* [16] *(initial* $c = [50, 100, 150, 200]$*, computational time* $= 73$ *seconds, segmentation accuracy* $= 98.94\%$*).*

to make the Chan–Vese algorithm more efficient, we use $|\nabla\phi_i|$ instead of $\delta_\epsilon(\phi_i)$ in the evolution equation, where ϕ_i are the level set functions.

7. Concluding remarks. In this paper we have proposed a new variational functional for multiphase image segmentation based on fuzzy region competition. We have shown the existence of minimizers of this functional and developed three methods to handle the constraints of membership functions of different regions. Numerical examples with grayscale and color images have shown that the three methods can provide similar image segmentation results, and their computational times are also about the same. By comparing with the Chan–Vese method (in two-phase and four-phase settings), the proposed methods are quite competitive and can provide very good image segmentation results. The three methods also have improved the hard partition algorithm by assigning membership function values to pixels in different regions. These membership function (fuzzy) values can be used to decide the core and uncertain pixels in the regions, thereby providing more useful information for dealing with fuzzy pixels. For instance, some of the pixels generated by the proposed method have membership function values that are not close to 0 or 1; see, for instance, Figures 2(h) and 3(d) in the two-phase segmentation and Figures 10(c)–10(f) in the four-phase segmentation.

In future work, we will consider the Mumford–Shah error function and the nonparametric error function. It is expected that these models can deal with more complex images such as low resolution medical images and texture images [19].

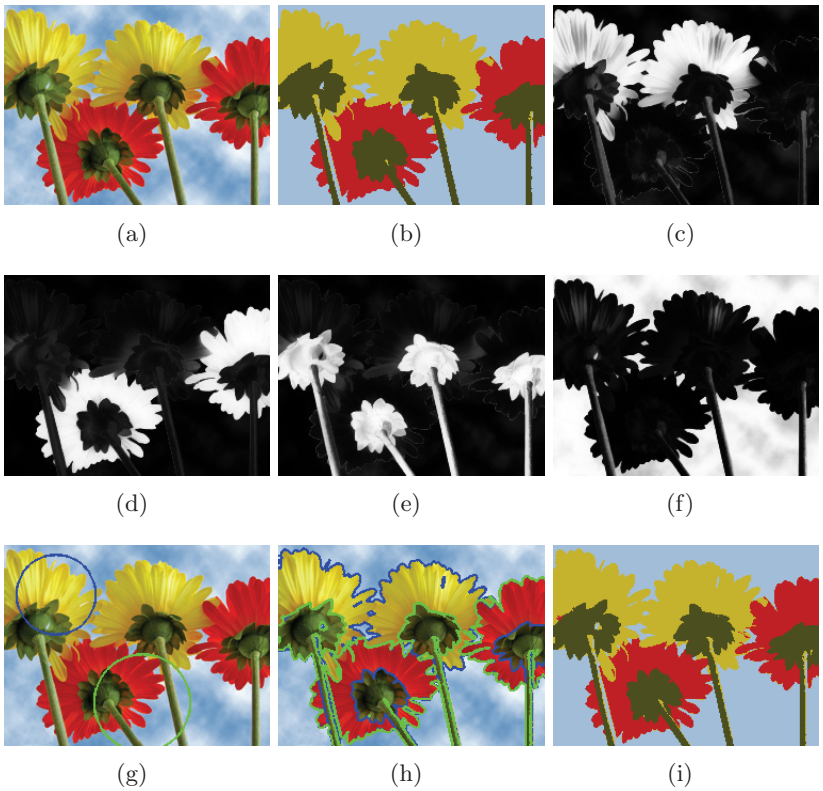

Figure 10. *Comparison of four-phase color image segmentation.* (a) *The test image is of size* 250×188; (b) *the piecewise constant image by Method* III *with* $\lambda = 0.002$; (c)–(f) *the membership functions* u_1, u_2, u_3, u_4 *(computational time* $= 7.1$ *seconds and number of iterations* $= 52$*);* (g) *the initial zero level sets;* (h) *the final zero level sets; and* (i) *the piecewise constant image by the Chan–Vese model (computational time* $= 14.5$ *seconds and number of iterations* $= 100$*).*

Acknowledgments. The authors would like to thank Profs. X.-C. Tai and E. Bae for the source code of [16]. The authors would also like to thank the referees for their useful suggestions to the manuscript.

REFERENCES

[1] G. Aubert and P. Kornprobst, *Mathematical Problems in Image Processing: Partial Differential Equations and the Calculus of Variations*, 2nd ed., Appl. Math. Sci. 147, Springer-Verlag, New York, 2006.

[2] J. C. Bezdek, L. O. Hall, and L. P. Clarke, *Review of MR image segmentation techniques using pattern recognition*, Med. Phys., 20 (1993), pp. 1033–1048.

[3] X. Bresson, S. Esedoḡlu, P. Vandergheynst, J.-P. Thiran, and S. Osher, *Fast global minimization of the active contour/snake model*, J. Math. Imaging Vision, 28 (2007), pp. 151–167.

[4] V. Caselles, R. Kimmel, and G. Sapiro, *Geodesic active contours*, Int. J. Comput. Vision, 1 (1997), pp. 61–79.

[5] T. F. Chan and L. A. Vese, *Active contours without edges*, IEEE Trans. Image Process., 10 (2001), pp. 266–277.

[6] T. F. Chan, S. Esedoḡlu, and M. Nikolova, *Algorithms for finding global minimizers of image segmentation and denoising models*, SIAM J. Appl. Math., 66 (2006), pp. 1632–1648.

[7] T. F. Chan, B. Sandberg, and L. Vese, *Active contours without edges for vector-valued images*, J. Visual Commun. Image Rep., 11 (2000), pp. 130–141.
[8] A. Chambolle, *An algorithm for total variation minimization and applications*, J. Math. Imaging Vision, 20 (2004), pp. 89–97.
[9] G. Chung and L. A. Vese, *Image segmentation using a multilayer level-set approach*, Comput. Vis. Sci., 12 (2009), pp. 267–285.
[10] N. Houhou, J. P. Thiran, and X. Bresson, *Fast texture segmentation model based on the shape operator and active contour*, in Proceedings of the IEEE Conference on Computer Vision and Pattern Recognition (CVPR 2008), IEEE Computer Society, Washington, DC, 2008, pp. 1–8.
[11] Y. Huang, M. K. Ng, and Y.-W. Wen, *A fast total variation minimization method for image restoration*, Multiscale Model. Simul., 7 (2008), pp. 774–795.
[12] Y. M. Jung, S. H. Kang, and J. Shen, *Multiphase image segmentation via Modica–Mortola phase transition*, SIAM. J. Appl. Math., 67 (2007), pp. 1213–1232.
[13] M. Kass, A. Witkin, and D. Tetzopoulos, *Snakes: Active contour models*, Int. J. Comput. Vision, 1 (1988), pp. 321–331.
[14] C. Li, C.-Y. Kao, J. C. Gore, and Z. Ding, *Implicit active contours driven by local binary fitting energy*, in Proceedings of the IEEE Conference on Computer Vision and Pattern Recognition (CVPR07), IEEE Computer Society, Washington, DC, 2007, pp. 1–7.
[15] J. Lie, M. Lysaker, and X.-C. Tai, *A binary level set model and some applications to Mumford-Shah image segmentation*, IEEE Trans. Image Process., 15 (2006), pp. 1171–1181.
[16] J. Lie, M. Lysaker, and X.-C. Tai, *A variant of the level set method and applications to image segmentation*, Math. Comp., 75 (2006), pp. 1155–1174.
[17] B. Mory and R. Ardon, *Fuzzy region competition: A convex two-phase segmentation framework*, in Scale Space and Variational Methods in Computer Vision (SSVM 2007), Lecture Notes in Comput. Sci. 4485, F. Sgallari, A. Murli, and N. Paragios, eds., Springer-Verlag, Berlin, Heidelberg, 2007, pp. 214–226.
[18] D. Mumford and J. Shah, *Optimal approximations by piecewise smooth functions and associated variational problems*, Comm. Pure Appl. Math., 42 (1989), pp. 577–685.
[19] N. Paragios and R. Deriche, *Geodesic active regions for supervised texture segmentation*, in Proceedings of the 7th International Conference on Computer Vision, Vol. 2, IEEE Computer Society, Washington, DC, 1999, pp. 926–932.
[20] C. Samson, L. B. Feraud, G. Aubert, and J. Zerubia, *A level set model for image classification*, Int. J. Comput. Vision, 40 (2000), pp. 187–197.
[21] J. A. Sethian, *Level Set Methods. Evolving Interfaces in Geometry, Fluid Mechanics, Computer Vision, and Materials Science*, Cambridge University Press, Cambridge, UK, 1996.
[22] J. Shen, *A stochastic-variational model for soft Mumford-Shah segmentation*, Int. J. Biomed. Imaging, (2006), Article ID 92329.
[23] L. A. Vese and T. F. Chan, *A multiphase level set framework for image segmentation using the Mumford and Shah model*, Int. J. Comput. Vision, 50 (2002), pp. 271–293.
[24] S. C. Zhu and A. Yuille, *Region competition: Unifying snakes, region growing, and Bayes/MDL for multiband image segmentation*, IEEE Trans. Pattern Anal. Mach. Intell., 18 (1996), pp. 884–900.